Journal of Materials Chemistry C

ROYAL SOCIETY OF CHEMISTRY

REVIEW

View Article Online
View Journal | View Issue

Cite this: J. Mater. Chem. C, 2020, 8, 11664

Single-crystal perovskite detectors: development and perspectives

Li Sun,[a] Wei Li,[a] Wei Zhu*[b] and Zhaolai Chen[c]

Visible-light and X-ray detectors based on semiconductors as light absorption and charge transport materials are widely used in image sensing, optical communication, biological detection, inspection, *etc.* Metal halide perovskite materials are promising candidates for visible-light and X-ray detectors due to their long carrier diffusion length, low trap density, strong absorption and tunable bandgap. Compared with the widely investigated polycrystalline thin films, single crystals exhibit better optoelectronic properties, showing potential for higher-performance detector devices. In this review, we will summarize the recent development of visible-light and X-ray detectors based on perovskite single crystals with different morphologies and device structures. The strategies to optimize the material properties and device performance will be discussed in detail. Finally, challenges and perspectives are proposed to promote further improvement in performance and practical application of single-crystal perovskite detectors.

Received 21st June 2020,
Accepted 21st July 2020

DOI: 10.1039/d0tc02944k

rsc.li/materials-c

1. Introduction

In the past decade, metal halide perovskites (MHPs) have drawn great attention towards optoelectronic applications[1–15] due to their superior properties, such as a high absorption coefficient,[16] unique defect physics,[17] long carrier recombination lifetime,[18] long carrier diffusion length,[19] and high charge mobility.[20] The molecular formula of MHPs is usually ABX_3, where A is a monovalent cation (such as methylammonium (MA^+), formamidinium (FA^+), Cs^+), B is a divalent metal ion (such as Pb^{2+} or Sn^{2+}), and X is a halide anion (such as I^-, Br^-, or Cl^-).[7] Since the first report by Miyasaka *et al.* in 2009,[21] perovskite solar cells have experienced a significant development with efficiency rocketing from 3.8% to 25.2%,[22] which is close to the silicon single crystal solar cells, showing great potential for commercial application. In addition to photovoltaic devices, MHP materials are also widely investigated in photodetectors,[23–25] X-ray detectors,[26] lasers,[27] light emitting diodes,[28–32] *etc.*

Polycrystalline thin films and single crystals are two popular forms of MHP materials for optoelectronic application. In general, polycrystalline thin films are obtained through spin-coating,[33–35] doctor-blading,[36] and vacuum deposition.[16,37,38]

[a] Department of Chemical Engineering, Zaozhuang Vocational College, Zaozhuang, 277800, China
[b] Institute of Radiation Medicine, Shandong Academy of Medical Sciences, Shandong First Medical University, Jinan, 250062, China. E-mail: fsszw@163.com
[c] State Key Laboratory of Crystal Materials, and Institute of Crystal Materials, Shandong University, No. 27 Shanda South Road, Jinan, 250100, China

Li Sun

Li Sun is an associate professor at the Department of Chemical Engineering, Zaozhuang Vocational College. She acquired her Master's degree in 2008 from the College of Chemistry and Chemical Engineering, Shandong University. Her current research interests focus on the synthesis of metal halide perovskite single crystals for photodetectors.

Wei Li

Wei Li is a professor at the Department of Chemical Engineering, Zaozhuang Vocational College. She acquired her Master's degree in 2010 from the College of Chemistry and Chemical Engineering, Shandong University. Her main research direction is functional crystal materials for optoelectronic devices.

These procedures can produce polycrystalline grains with sizes from several hundreds of nanometers to several micrometers. That is to say, large amounts of grain boundaries which are rich in charge traps exist in the polycrystalline thin films,[39–41] which is adverse to the optoelectronic properties[42–44] and the stability of the perovskite materials.[45] In comparison, MHP single crystals are free of grain boundaries and have been demonstrated with lower defect density, better optoelectronic properties and higher stability than the polycrystalline thin films.[46–57] Dong *et al.* observed an ultra-low trap state density of 10^{10} cm^{-3} and an ultra-long charge carrier diffusion length of 175 μm under one sun illumination in methylammonium lead iodide ($MAPbI_3$) single crystals.[58] Chen *et al.* reported that mixed cation and mixed halide perovskite single crystals remained stable even after 10 000 h of water–oxygen and 1000 h of light aging.[59] Besides, the absorption spectrum of MHP single crystals red shifts obviously, which can broaden the photoresponse of single-crystal perovskite solar cells, thus increasing the upper limit of short-circuit current density and power conversion efficiency.[14] In fact, it has been universally recognized that perovskite single crystals are promising for higher-performance and more stable optoelectronic devices.

Currently, the superior properties of perovskite single crystals have endowed perovskite photodetectors and X-ray detectors with excellent device performance, while the single-crystal solar cells and light emitting diodes still lag far behind the polycrystalline counterpart. For example, Huang *et al.* found that X-ray detectors made of methylammonium lead bromide ($MAPbBr_3$) perovskite bulk single crystals showed ultra-high sensitivity, which was four times higher than the sensitivity achieved with commercial α-Se X-ray detectors.[60] Zhang *et al.* reported visible-light photodetectors based on formamidinium lead dibromide ($FAPbBr_3$) micro single crystals with a specific detectivity of 3.87×10^{14} Jones.[61] The obtained high performance indicates that MHP single crystals have great potential for practical applications in detection, imaging, and communication, although there are still some obstacles that are to be overcome.

In this review, the recent development of photodetectors and radiation detectors based on perovskite single crystals will be summarized. The strategies to optimize the material properties and device performance will be discussed in detail. Finally, challenges and perspectives are proposed to promote further improvement in performance and practical application of single-crystal perovskite detectors.

2. Single-crystal perovskite photodetectors

Photodetectors are devices that can convert light signals to electrical signals *via* the photoelectric effect, which have a broad range of applications, including image sensing, optical communication, environmental monitoring, and chemical/biological detection, in both academic and industrial domains.

In 2015, the $MAPbI_3$ bulk single crystal was synthesized using three independent groups and used to investigate the intrinsic property of perovskites.[58,62,63] Due to the superior optoelectronic properties and large thickness, the bulk perovskite single crystal was first investigated for its use in photoconductor-type photodetectors (Fig. 1a).[64] Subsequently, Bakr *et al.* found that the micro single crystal integrated with the patterned substrate can increase the detector performance significantly.[65] The photoconductor-type photodetectors usually show high responsivity and specific detectivity, but slow

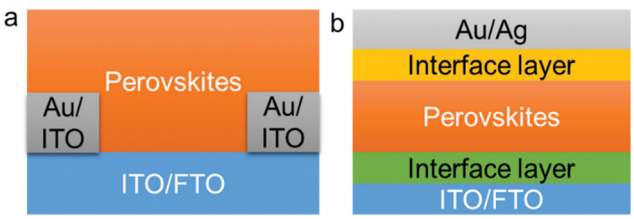

Fig. 1 Schematic for perovskite-based photodetectors. (a) The photoconductors and (b) the photodiodes.

Zhu Wei

Wei Zhu is an assistant researcher at the Institute of Radiation Medicine, Shandong Academy of Medical Sciences, Shandong First Medical University. He acquired his bachelor's degree in 2002 at Shandong University and Master's degree in 2005 from the Shandong Academy of Medical Sciences. His research interests focus on radiation effects and radiation detection-related materials.

Zhaolai Chen

Zhaolai Chen is currently a professor at the State Key Lab of Crystal Materials and Institute of Crystal Materials, Shandong University. He received his bachelor's degree in 2011 and PhD in 2016 under the supervision of Prof. Bai Yang at Jilin University. He then conducted postdoctoral research at the University of Nebraska–Lincoln and the King Abdullah University of Science and Technology. His current research interests focus on the design and synthesis of metal halide perovskite single crystals for solar cells, photodetectors, and X-ray detectors.

response speed. To achieve a fast response, Huang *et al.* grew thickness-controlled single crystal thin films to fabricate photodiode-type photodetectors (Fig. 1b).[66] In this section, key parameters characterizing the performance of the photodetector are introduced briefly. Subsequently, two kinds of photodetectors based on perovskite single crystals with different morphology will be introduced, and the strategies to improve device performance will be discussed.

The key performance parameters of photodetectors include responsivity, detectivity, noise, a linear dynamic range, and response speed:

(1) Responsivity (R): indicates the response efficiency of photodetectors to optical signals. It is expressed as:

$$R = \frac{J_{ph}}{L_{light}}$$

where J_{ph} is the photocurrent and L_{light} is the incident-light intensity. Because R is proportional to the external quantum efficiency (EQE) of the photodetector, it can also be expressed as

$$R = \frac{EQE \cdot \lambda q}{hc}$$

where λ is the incident-light wavelength, q is the absolute value of electron charge, h is the Planck constant, and c is the speed of light.

(2) Detectivity (D^*): indicates the weakest level of light that the device can detect. It can be written as

$$D^* = \frac{(A\Delta f)^{1/2} \cdot R}{i_n}$$

where A is the effective area of the photodetector, Δf is the electrical bandwidth, and i_n is the noise current.

(3) Noise equivalent power (NEP): means that the photodetector can distinguish the minimum impinging optical power of noise. It can be written as:

$$NEP = \frac{(A\Delta f)^{1/2}}{D^*} = \frac{i_n}{R}$$

(4) Linear dynamic range (LDR): it describes a range of illumination intensity in which the current response of the photodetector is linearly proportional to the light intensity. It is expressed as

$$LDR = 20 \log \frac{J_{upper} - J_d}{J_{lower} - J_d}$$

where J_{upper} is the current value of the device's response deviating from linearity, J_{lower} is the lower resolution limit, and J_d is the dark current.

(5) Response speed: is defined as the time between 10% and 90% of the maximum photocurrent. It is closely related to charge transport and collection. The smaller the electrode spacing (charge carrier path length), the more conducive the rapid response is.

2.1 Photoconductor-type photodetectors

In photoconductor-type photodetectors, photo-generated carriers shuttle between two electrodes before recombination, showing an intrinsic photocurrent amplification phenomenon.[67] The photocurrent gain is proportional to the carrier lifetime and carrier mobility, but is inversely proportional to channel width. Therefore, the high carrier mobility and long carrier lifetime can endow photoconductors with high photocurrent gain, and thus high responsivity and detectivity. Besides, shortening the channel width is also a useful way to increase the performance parameters.

2.1.1 Photoconductors based on bulk single crystals. Lian *et al.* reported the first photoconductors based on the (100) facet of the $MAPbI_3$ bulk single crystal, which showed much better performance than the device based on polycrystalline thin films (Fig. 2).[64] By using a simple Au/$MAPbI_3$/Au planar structure, they obtained a high responsivity of 953 A W^{-1} and an external quantum efficiency (EQE) of 2.22 × 10^5% at 1 V bias when illuminated with 532 nm light of 2.12 nW cm^{-2} (Fig. 2c and d). In addition, the single crystal photodetectors were found to exhibit good stability and a relatively fast response speed of 58 μs (Fig. 2e and f). The crystal quality correlates intimately with the carrier lifetime and mobility; therefore, optimizing the crystal growth is important to improve the detector performance. Liu *et al.* developed a low-temperature-gradient crystallization approach to grow $MAPbBr_3$ single crystals (Fig. 3a and b).[53] This method improves the carrier mobility,

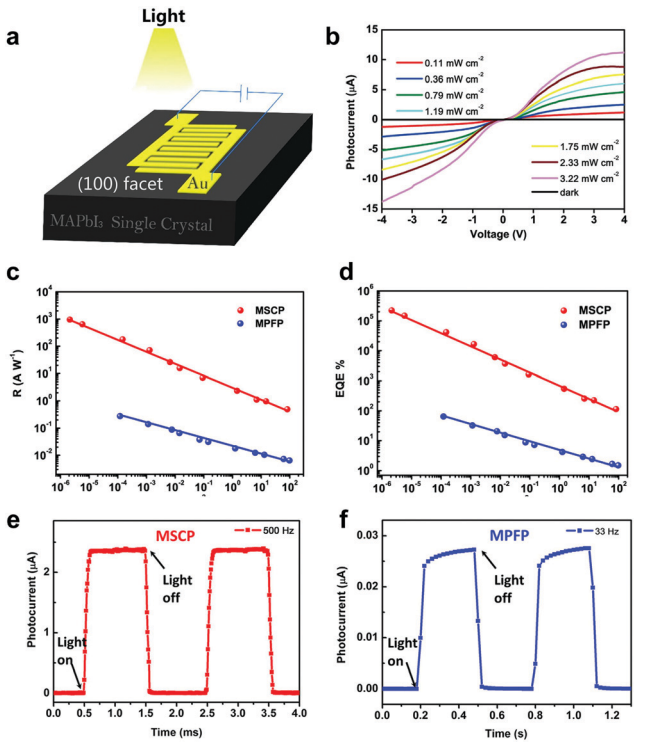

Fig. 2 (a) Schematic diagram of the planar-type photodetector fabricated on the (100) facet of a $MAPbI_3$ single crystal. (b) Photocurrent *versus* voltage curves under different irradiation conditions. (c) Responsivity R *versus* irradiance power curves. (d) External quantum efficiency EQE *versus* irradiance power curves. (e) Transient photocurrent response for the MSCP with on-and-off light with a switching frequency of 500 Hz. (f) Transient photocurrent response for the MPFP with a switching frequency of 33 Hz. Reproduced with permission.[64] Copyright 2015, Springer Nature.

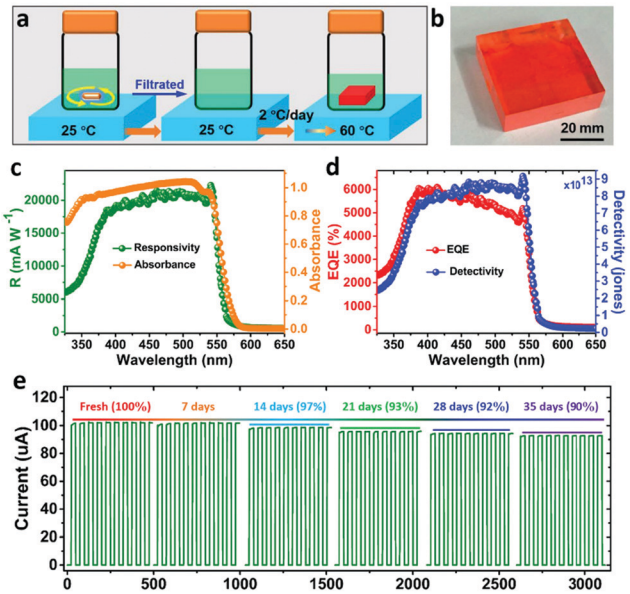

Fig. 3 (a) Schematic diagram for the LTGC crystallization process of the $MAPbBr_3$ single crystals. (b) Photograph of $MAPbBr_3$ single crystals grown *via* the LTGC process. (c) Responsivity (R) and absorbance of the $MAPbBr_3$ single crystal photosensor. (d) External quantum efficiency (EQE) and detectivity (D^*) of the $MAPbBr_3$ single crystal photosensor. (e) Photoresponse stability measured on the $MAPbBr_3$ single crystal photosensor under 525 nm illumination. The photoresponse was periodically measured for an exposure time of 35 days in ambient air with the humidity level at ≈50% RH. Reproduced with permission.[53] Copyright 2018, Wiley-VCH.

carrier lifetime and crystal uniformity obviously. As a result, the as-fabricated photodetectors with a device structure of Au/$MAPbBr_3$/Au showed very high responsivity, EQE, and a specific detectivity of 6×10^{13} Jones (Fig. 3c and d). Besides, the photodetectors show excellent stability with 90% current density after 35 days of storage (Fig. 3e). Interestingly, the photodetectors show very homogeneous photocurrent and dark current, therefore, a large-area (≈1300 mm^2) imaging assembly composed of a 729-pixel sensor array was constructed, showing excellent imaging capability (Fig. 4). In addition to crystal quality, another possible factor determining the detector performance is the device fabrication technique, considering the very simple metal/perovskite/metal structure. As perovskite materials are delicate, the surface can be readily damaged by the high-energy atom bombardment and strong local heating during vacuum-deposition. Single-crystal perovskite photodetectors are also useful for fundamental investigation, such as facet-dependent optoelectronic properties.[82] Ding *et al.* fabricated photodetectors on the (220) and (100) facets of $MAPbI_3$ single crystals.[82] The experimental results revealed a large anisotropy of optoelectronic properties between (220) and (100) facets, which was interpreted in terms of surface structures and ion migrations.

2.1.2 Photoconductors based on micro single crystals. Perovskite bulk single crystals are usually free-standing and are difficult to integrate with a substrate. In comparison, perovskite micro single crystals with sizes of tens of micrometers showed fast growth, superior optoelectronic properties, capability for large-area production, and easy integration with a substrate.

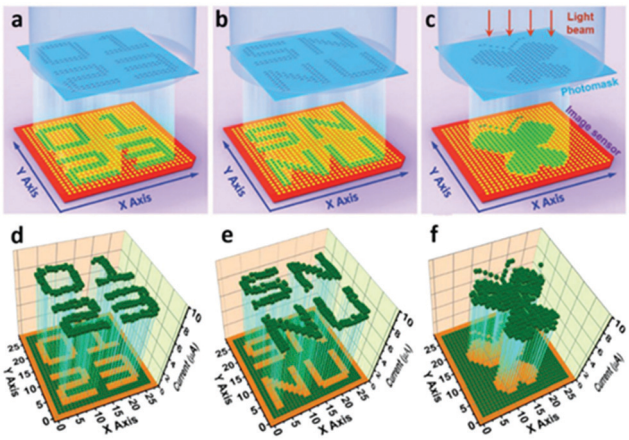

Fig. 4 (a–c) Schematic diagram for the projection imaging mechanism. A prepatterned photomask was used directly above the imaging assembly. Under light illumination, the optical pattern is projected onto the sensor unit with a contrast of light and dark through the mask to form a mask image. (d–f) The corresponding photocurrent outputs from each pixel with different optical patterns of "0123," "SNNU," and a butterfly. Reproduced with permission.[53] Copyright 2018, Wiley-VCH.

To obtain micro-single crystals, perturbation by stirring or sonicating is essential to introduce multi crystal nuclei.[65] Saidaminov *et al.* first reported the fabrication of large-area $MAPbBr_3$ microcrystal films by stirring on the pre-patterned ITO substrate with the channel width of 5 μm (Fig. 5a and b).[65] The $MAPbBr_3$ microcrystal showed a size of 30–50 μm, a carrier mobility of 60 $cm^2\ V^{-1}\ s^{-1}$, a carrier lifetime of 189 ns, a trap density of $2 \times 10^{11}\ cm^{-3}$, and a carrier diffusion length of 5 μm, which slightly lagged behind the $MAPbBr_3$ bulk single crystal (Fig. 5c and d). Using a simple structure of ITO/$MAPbBr_3$/ITO, the as-fabricated photodetectors showed very high performance with a responsivity of 4000 $A\ W^{-1}$ (Fig. 5e) and a response speed of 25 μs. In spite of the relatively poor properties, the performance of the photodetectors is much better than the photodetectors based on the $MAPbBr_3$ bulk single crystal with a similar structure. This should be attributed to the 10-fold smaller channel width and the prevention of damage of the brittle perovskite during the vacuum-deposition of metal electrodes. By controlling the microcrystal thickness, Saidaminov *et al.* achieved broadband and narrowband detection simultaneously in this simple structure.[68] The as-fabricated photodetectors exhibited a broadband response upon illumination from the ITO side while they exhibited a narrowband response upon illumination from the air/perovskite side. Adinolfi *et al.* extended this structure to the $MAPbCl_3$ microcrystal and achieved high-performance visible-blind UV photodetectors with a responsivity of 18 $A\ W^{-1}$, a specific detectivity of 10^{12} Jones, and a response speed of 1 ms.[69] Zhang *et al.* reported ultrahigh-performance visible-light photodetectors based on $FAPbBr_3$ microcrystals with a responsivity of 4000 $A\ W^{-1}$, an EQE of 10^6%, a specific detectivity of 3.87×10^{14} Jones, and a response speed of 0.75 ms.[61] The higher performance is due to the better optoelectronic properties of FA-based perovskites, indicating that the FA-based perovskite is an excellent candidate for highly sensitive and fast photodetectors.

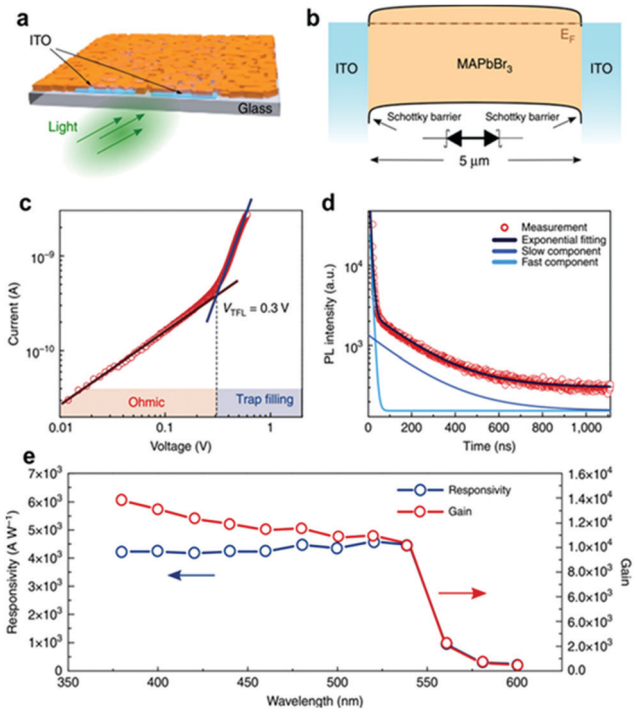

Fig. 5 (a) Three-dimensional diagram of the photodetector: the $MAPbBr_3$ ISC perovskite layer (orange) is deposited on top of the ITO contacts (light blue). The detector is placed on a glass substrate (transparent gray). (b) Energy diagram of the photodetector. (c) *I–V* characteristic of the $MAPbBr_3$ ISC perovskites. (d) PL time decay trace at λ = 560 nm. (e) Responsivity and gain of the photodetector. Reproduced with permission.[65] Copyright 2015, Springer Nature.

2.1.3 Photoconductors based on single crystal thin films. Based on the principle of photoconductor-type photodetectors, small channel width can lead to higher responsivity and photocurrent gain. For both bulk and micro single crystals, it is challenging to construct sub-micrometer channels using a relatively cheap vacuum deposition technique. In this case, a single crystal thin film provides a way to adjust the channel width down to sub-micrometer by controlling the film thickness. The most popular method for obtaining single crystal thin films is the space-confined method in which the vertical crystal growth is limited by the substrates.[14] The crystals can only grow along the lateral direction, thus generating single crystal thin films. Yang *et al.* grew a $MAPbBr_3$ single crystal thin film with the thickness of hundreds of nanometers using the space-confined method with the assistance of external pressure.[70] Then they deposited two electrodes on the opposite side of the as-grown single crystal thin film to construct a vertical-structure photodetector; in this case, the crystal thickness is the channel width. By using the sub-micrometer channel, they obtained a record photocurrent gain of 50 million and a gain-band-width product of 70 GHz (Fig. 6). The crystal size using the space-confined method is usually several millimeters or hundreds of micrometers, which limits their practical application.[14] To obtain large-area single crystal thin films, Liu *et al.* developed the top-down method in which bulk single crystals were first grown and then sliced into thin wafers.[83] But the thickness using the top-down method can hardly go down below 100 μm.

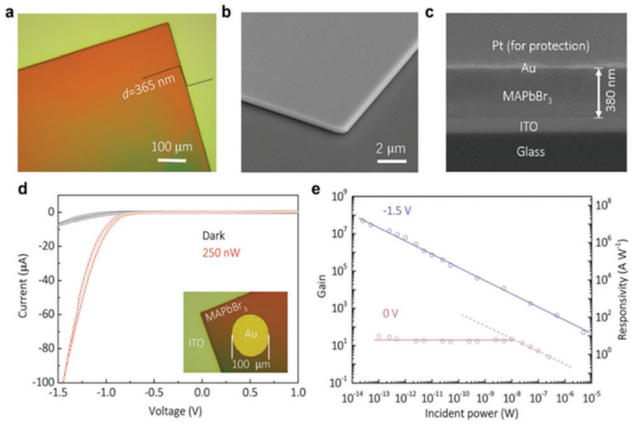

Fig. 6 (a) Optical image of a single-crystal perovskite thin film. (b) SEM image of a single-crystal perovskite thin film. (c) SEM image of the cross section of photodetectors based on single-crystal perovskite films. (d) *I–V* curves in forward and backward sweeping directions of a photodetector. (e) Gain and responsivity of the device. Reproduced with permission.[70] Copyright 2018, Wiley-VCH.

2.1.4 Photoconductors based on low-dimensional perovskite single crystals. For the photoconductors based on perovskite single crystals, one challenge is ion migration induced by an electrical field, which generates large dark current, and thus leads to high noise and low detectivity. For the widely-investigated three-dimensional perovskites, ion migration can be suppressed in single crystals, but is still inevitable. Recently, Huang *et al.* reported that the activation energy of ion migration increased a lot in two-dimensional perovskites due to reduced ion vacancy, compared to three-dimensional perovskites.[71] The suppressed ion migration in two-dimensional perovskite single crystals can lead to low dark current, thus leading to high detectivity. Liu *et al.* fabricated photoconductors based on a high-quality, flexible, two-dimensional single crystal: $(C_6H_5CH_2CH_2NH_3)_2PbI_4$ (Fig. 7a–c).[72] Although the photoconductors exhibit a moderate responsivity of 98.17 A W^{-1}, the very low dark current leads to an ultralow noise of 9.18 $\times$ 10^{-16} A $Hz^{-1/2}$ and an ultrahigh detectivity of 1.62 $\times$ 10^{15} cm $Hz^{1/2}$ W^{-1} (Fig. 7d–f). The detectivity is one to two orders of magnitude higher than those based on three-dimensional single crystals.

2.2 Photodiode-type photodetectors

Another kind of photodetectors based on the perovskite single crystals is photodiode-type, in which a sandwiched structure with two asymmetrical electrodes is used.[67] The biggest advantage of photodiode-type photodetectors is their fast response speed, which shows great potential for light communication, fast detection, *etc.* Besides, the existence of electron and hole transport layers results in electrons and holes being collected selectively, thus leading to no photocurrent gain and low dark current. Therefore, photodiode-type photodetectors usually show lower responsivity and noise than the photoconductor-type photodetectors.

2.2.1 Photodiodes based on bulk single crystals. Maculan *et al.* first reported a visible-blind UV photodetector based on a $MAPbCl_3$ bulk single crystal with a vertical device structure:

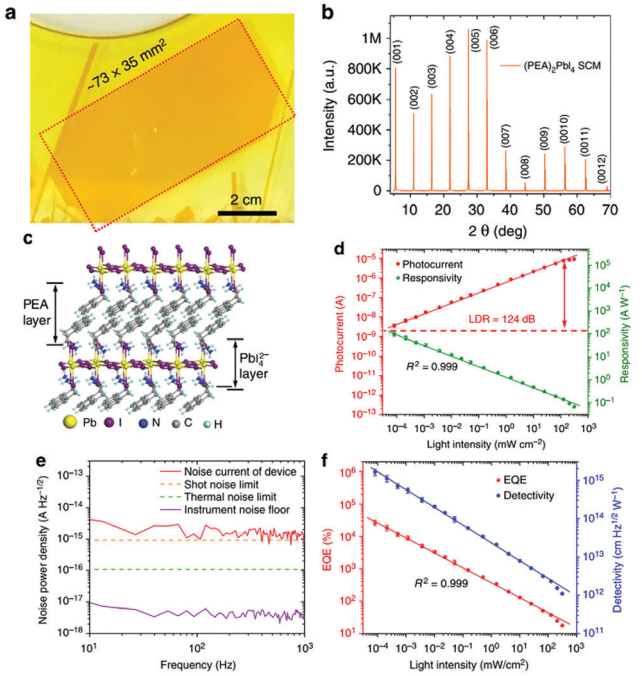

Fig. 7 (a) Photo of the $(PEA)_2PbI_4$ SCM sample. (b) XRD pattern of the $(PEA)_2PbI_4$ SCM photosensors. (c) Layered crystal structure of $(PEA)_2PbI_4$. (d) Photocurrent and responsivity of the $(PEA)_2PbI_4$ SCM photosensors. (e) Dark current noise at different frequencies of the $(PEA)_2PbI_4$ SCM photosensor. (f) EQE and D^* of the $(PEA)_2PbI_4$ SCM photosensor. Reproduced with permission.[72] Copyright 2018, Springer Nature.

Pt/$MAPbCl_3$/Ti/Au (Fig. 8a and b).[73] The $MAPbCl_3$ single crystal was grown using the inverse temperature crystallization (ITC) method involving the DMF–DMSO mixed solution. The as-grown single crystal exhibited superior properties, including a high carrier mobility of 42 $cm^2\ V^{-1}\ s^{-1}$, a long carrier lifetime of 662 ns, and a low trap density of $3.1 \times 10^{10}\ cm^{-3}$. The limited absorption range of the single crystal made it a good candidate for visible-blind UV photodetectors. The as-fabricated UV photodetectors showed a current on/off of 1100, a responsivity of 46.9 mA W^{-1}, a specific detectivity of 1.2×10^{10} Jones, and a response speed of 24 ms (Fig. 8c and d). Compared to the organic–inorganic hybrid perovskite, all inorganic perovskites show better stability, but do not deteriorate the optoelectronic properties. Saidaminov *et al.* developed a rapid, low-temperature, solution-based phase-selective synthesis of millimeter-sized cesium lead bromide bulk single crystals of millimeter-sized cesium lead bromide bulk single crystals with different compositions, including $CsPbBr_3$, Cs_4PbBr_6, and $CsPb_2Br_5$.[74] A higher ON/OFF ratio of 10^5 and a response time of 60 ms were obtained for self-powered visible-light detectors based on millimeter-sized $CsPbBr_3$ single crystals.

The large thickness of the bulk single crystal and the existence of surface charge traps could be used to construct narrowband photodetectors. Fang *et al.* synthesized a series of perovskite bulk single crystals with the absorption edge continuously tuned from blue to red.[75] The photogenerated carriers were mainly located close to the surface of the single crystal upon excitation by short-wavelength light, and the carriers could not be collected due to the strong recombination assisted by the surface charge traps.

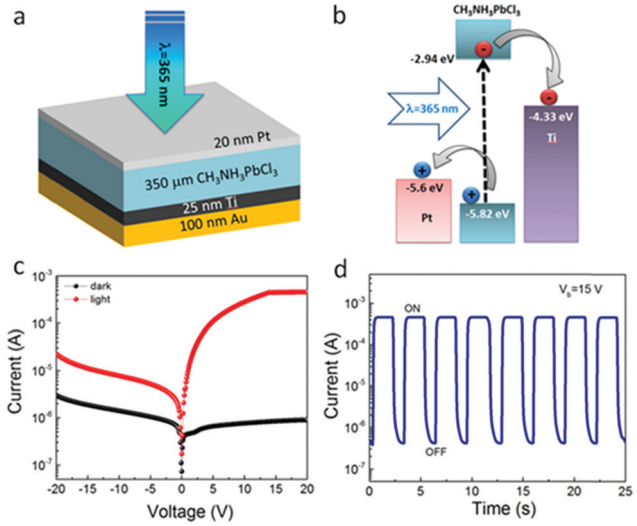

Fig. 8 (a) Device structure of the MAPbCl3 single crystal photodetector. (b) Energy band diagram. (c) *I*–*V* curves of the photodetector under illumination. (d) ON–OFF photoresponse under modulated UV illumination. Reproduced with permission.[73] Copyright 2015, American Chemical Society.

In contrast, the carriers generated by below-bandgap excitation distributed across the whole single crystal, which can be partly transported and collected by the electrode, leading to a photo response at the band edge position. A very narrow spectrum response with a full-width at half-maximum of smaller than 20 nm was obtained and the peak position of EQE could be adjusted by controlling the composition of the perovskite single crystals (Fig. 9).

2.2.2 Photodiodes based on single crystal thin films. The large thickness of bulk single crystals causes a very long carrier transit time, leading to a slow response speed. To reduce the response time, Bao *et al.* grew millimeter-sized $MAPbI_3$ and $MAPbBr_3$ single crystal thin films with a thickness of 10 μm by developing a hydrophobic interface confined lateral crystal growth method.[66] A photodetector with a p–i–n structure was constructed: ITO/PTAA/single crystal thin film/C_{60}/BCP/Cu (Fig. 10a). The absence of grain boundaries and pinholes suppressed the dark current effectively, leading to a very low noise current of 1.4 fA $Hz^{-1/2}$ (Fig. 10b), a low detection limit of 0.35 pW cm^{-2} (Fig. 10f), and a high specific detectivity of 1.5×10^{13} Jones (Fig. 10e). Benefitting from the small thickness and large mobility of the $MAPbI_3$ and $MAPbBr_3$ single crystal thin films,

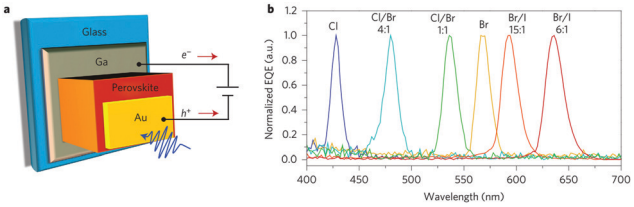

Fig. 9 (a) Schematic diagram of the device structure. (b) Normalized EQE spectra of the single-halide and mixed-halide perovskite single-crystal photodetectors. Reproduced with permission.[75] Copyright 2015, Springer Nature.

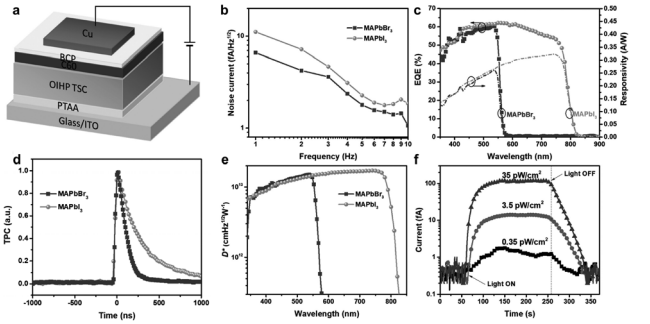

Fig. 10 (a) Schematic architecture of the photodetector based on perovskite TSCs. (b) Noise current of photodetectors based on perovskite TSCs. (c) EQE and responsivity spectra of photodetectors based on perovskite TSCs. (d) Transient photocurrent of photodetectors based on perovskite TSCs. (e) Specific detectivity (D^*) of devices based on perovskite TSCs. (f) Current output of the MAPbBr3 TSC device to green light. Reproduced with permission.[66] Copyright 2017, Wiley-VCH.

high response speeds of 296 ns and 100 ns were obtained (Fig. 10d). Xiao *et al.* subsequently demonstrated that the response speed of the $MAPbI_3$ single crystal thin film photodetectors was mainly limited by the slow trapping/detrapping processes induced by the surface charge traps.[76] The effective passivation of the surface charge traps by argon plasma treatment resulted in a 100-fold increase in the response speed from 1.5 μs to 15 ns for the photodetectors based on $MAPbI_3$ single crystal thin films with a thickness of 15 μm. Based on a carrier mobility of 150 $cm^2\ V^{-1}\ s^{-1}$ and a build-in potential of 1 V, the carrier transit time in this device was estimated to be about 15 ns, consistent with the measured response time, indicating that the response time was only limited by the transit time. Therefore, reducing thickness down to below 10 μm, which is still a big challenge for lead-iodide perovskite single crystals, is required to further increase the response speed in the future.

The photo response range of perovskite materials can be controlled by changing the halide ions. Chen *et al.* achieved visible-blind UV photodetectors with nanosecond response time and high detectivity based on $MAPbCl_3$ single crystal thin films.[49] When using a $MAPbCl_3$ crystal with a thickness of 1 μm, the response time of 15 ns was obtained for the visible-blind UV photodetectors, which was several orders of magnitude faster than the ever-reported solution-processed visible-blind UV photodetectors and is comparable to the reported UV photodetectors based on traditional inorganic semiconductors.

3. X-ray detectors

Radiation detectors are widely used in medical imaging, dosimeters, photon counters, spectroscopy, and nuclear reaction monitors. When X-ray detectors are applied for dosimeter or medical imaging, they work in a current mode. In this mode, multiple photons arrive at the semiconductor detector together, and an X-ray photon can be converted directly *via* the photoelectric effect process into many excess free charges within the semiconductor, which are then collected by the electrode under bias. When the radiation detectors are applied for photon counters, spectroscopy, and nuclear reaction monitor, they work in a voltage mode. Contrary to the current mode, photons arrive at the detector one by one. Each photon generates some electron–hole pairs, and the corresponding charge number is calculated in the signal pulse, and its intensity is proportional to the energy of the photon. The γ-ray photon energy spectrum can be drawn by using the histogram directivity of photon energy.[77]

Compared with other semiconductor materials, the single-crystal perovskite has the following advantages, which makes it have excellent performance in the radiation detector.

(1) It has a strong stopping power and therefore provides a large linear attenuation coefficient.

(2) It presents much lower trap density and improved crystallinity due to the freeing of the grain boundaries of polycrystals, therefore it has a large mobility–lifetime (μ–τ) product.

(3) It has large bulk resistivity, resulting in the radiation detectors having small dark current and noise.

(4) It has relatively better tolerance to defects than other semiconductor materials, and therefore it possesses radiation hardness.

3.1 X-ray detectors based on lead perovskite single crystals

Wei *et al.* first reported a sensitive X-ray detector made of the methylammonium lead bromide ($MAPbBr_3$) perovskite bulk single crystal.[60] A record $\mu\tau$ product of $1.2 \times 10^{-2}\ cm^2\ V^{-1}$ was obtained by using a non-stoichiometry precursor for crystal growth, thus ensuring effective carrier transport and suppressing the undesired dark current by lowering the applied bias. Besides, the carrier lifetime and extraction efficiency were increased by decreasing the surface charge recombination velocity with UV-O_3 treatment. Finally, the as-fabricated single crystal devices showed a detectable X-ray dose rate as low as 0.5 $\mu Gy_{air}\ s^{-1}$ with a sensitivity of 80 $\mu C\ Gy_{air}^{-1}\ cm^{-2}$ (Fig. 11), which was four times higher than the sensitivity achieved with α-Se X-ray detectors. Subsequently, the same group reported the monolithic integration of the $MAPbBr_3$ single crystal onto the silicon substrate through a facile, low-temperature, solution-processed molecular bonding.[26] The dipole of the bonding molecule reduced device noise at high bias, but retained the signal intensity, resulting in a much higher sensitivity of $2.1 \times 10^4\ \mu C\ Gy_{air}^{-1}\ cm^{-2}$ and a much lower detection limit of 0.1 $\mu Gy_{air}\ s^{-1}$ under 8 keV X-ray radiation.

3.2 X-ray detectors based on lead-free perovskite single crystals

In spite of the low-cost fabrication and outstanding performance demonstrated with the lead-based single crystal X-ray detectors, they face a big problem: lead is toxic. To solve this problem, Pan *et al.* reported the synthesis of the $Cs_2AgBiBr_6$ perovskite bulk single crystal and its application in X-ray detectors.[78] $Cs_2AgBiBr_6$ has an average Z value of 53.1, which is higher than $MAPbI_3$ (Z = 48.9) and $MAPbBr_3$ (Z = 45.1), thus showing a higher X-ray absorption coefficient (Fig. 12a).

The thermal annealing treatment of the $Cs_2AgBiBr_6$ single crystal at 373 K in nitrogen for 2 h led to a high $\mu\tau$ product of $3.75 \times 10^{-3}\ cm^2\ V^{-1}$ and a low surface recombination velocity

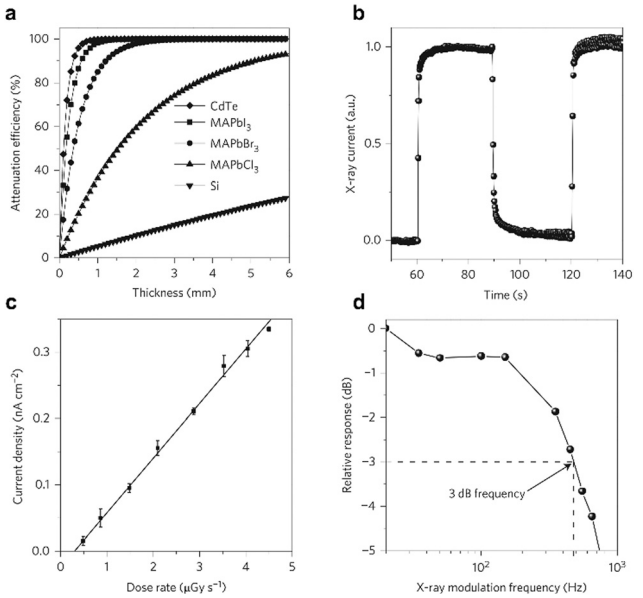

Fig. 11 (a) Attenuation efficiency of CdTe, $MAPbI_3$, $MAPbBr_3$, $MAPbCl_3$ and silicon to 50 keV X-ray photons *versus* thickness. (b) $MAPbBr_3$ single-crystal device response to X-rays by turning the X-ray source on and off. (c) X-ray-generated photocurrent at various dose rates, down to the lowest detectable dose rate. (d) Normalized response as a function of input X-ray frequency showing that the 3 dB cutoff frequency is 480 Hz. Reproduced with permission.[60] Copyright 2016, Springer Nature.

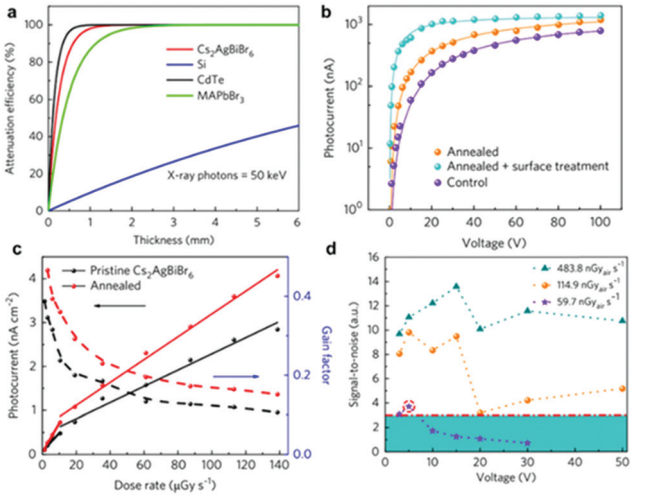

Fig. 12 (a) Attenuation efficiency of various semiconductors to 50 keV X-ray photons *versus* thickness. (b) Bias-dependent photoconductivity of $Cs_2AgBiBr_6$ SCs. (c) X-ray photocurrents and gain factor *versus* dose rate. (d) Signal-to-noise ratio of the device. Reproduced with permission.[78] Copyright 2017, Springer Nature. Attenuation efficiency of various semiconductors to 50 keV X-ray photons *versus* thickness. (b) Bias-dependent photoconductivity of $Cs_2AgBiBr_6$ SCs. (c) X-ray photocurrents and gain factor *versus* dose rate. (d) Signal-to-noise ratio of the device. Reproduced with permission.[78] Copyright 2017, Springer Nature.

of 1496 cm s^{-1} (Fig. 12b). Moreover, the suppressed ion migration in $Cs_2AgBiBr_6$ inhibited the dark current obviously, thus permitting the single crystal X-ray detectors work at a relatively larger external bias. Efficient charge collection was therefore guaranteed without a substantial increase in noise current. Finally, the detection limit as low as 59.7 nGy_{air} s^{-1} was obtained, which was comparable to the lead-based single crystal X-ray detectors (Fig. 12c and d). After $Cs_2AgBiBr_6$ single crystals, a series of lead-free perovskite single crystals were reported for X-ray detectors, such as $MA_3Bi_2I_9$,[79] $Rb_3Bi_2I_9$,[80] $C_3Bi_2I_9$,[81] *etc.*

4. Challenges and perspectives

Different from solar cells and light emitting diodes, photodetectors and X-ray detectors based on MHP single crystals have achieved better performance than those based on polycrystalline thin films. And their performance can be further improved by optimizing material properties and the device fabrication technique. Besides, investigation of single-crystal detector applications is rarely reported, in spite of their better performance. To provide guidelines for the future development of single-crystal photodetectors and their applications, we highlight the following challenges and perspectives.

(1) Many reports confirm the existence of a large amount of charge traps on the surface of perovskite single crystals, which causes a high surface charge recombination rate. For photoconductor-type photodetectors, the carriers are mainly travelled in the surface part of perovskite single crystals. For photodiode-type photodetectors, the trapping–detrapping process of carriers will increase the response time. For X-ray detectors, the surface charge traps are adverse to the interface carrier transport, and therefore this increases the bias and dark current. Therefore, for both photodetectors and radiation detectors, their performance correlates intimately with surface charge recombination. The loss of organic amine ions and halide ions is the main reason causing high surface charge trap density in perovskite single crystals. Therefore, developing effective methods to replenish the organic component will increase the material property and device performance. Possible strategies to replenish the organic iodide are proposed as follows: treatment of the single crystal with organic iodide vapor, spin coating the organic iodide solution, immersing the single crystal in the organic iodide solution.

(2) For photoconductor-type photodetectors, current device fabrication processes usually include the vacuum deposition of gold electrodes directly on the surface of perovskite single crystals. However, the perovskite materials are delicate and can be readily damaged by the high-energy atom bombardment and strong local heating during the vacuum-deposition of the metal electrode, which may be detrimental to the charge transport across the metal/perovskite interface and the photodetector performance. Developing new techniques to deposit the electrode without damaging the perovskite materials, such as lamination processes, may further improve the performance of the single-crystal perovskite photoconductors.

(3) For photodiode-type photodetectors, it is still challenging to reduce the response time to sub-nanosecond, which has important applications in light communication, fast detection, *etc.* Current methods to grow millimeter-sized perovskite single crystal thin films usually lead to a crystal thickness of larger

than 10 μm. Developing a novel method to further reduce the crystal thickness to be comparable to the polycrystalline thin film is an urgent question to be solved, which will benefit the development of single-crystal solar cells. Besides, reducing the crystal thickness will lead to an obvious increase in the device capacitance, and thus result in the resistance–capacitance (RC) constant, which is in conflict with the reduced transit time. Therefore, these two factors should be considered simultaneously to achieve the sub-nanosecond response time.

(4) Although the performance of X-ray detectors based on bulk single crystals is excellent, these results only satisfy the requirement of single-element detector applications, such as X-ray dosimetry. For medical radiography and many other X-ray-based imaging techniques, the integration of these single crystals on the commercial chip with two-dimensional pixels is necessary. The conflict between the flat surface of the single crystal and the microstructure of the chip may be a potential challenge for the integration, which may be solved by using the microcrystals with smaller size and similar optoelectronic properties. Besides, the large thickness and high carrier mobility of the bulk single crystal may cause difficult differentiation between the adjacent pixels. To solve this problem, a large-area thin single crystal wafer can be used to further increase the resistivity of single crystals to make them sustain high bias.

5. Conclusions

The superior optoelectronic properties of perovskite single crystals make them excellent candidates for detectors. Currently, X-ray detectors based on bulk single crystals shows better performance than those based on commercial α-Se. The optimization of single crystal thin films with different thickness and crystal quality has led to the highest photocurrent gain in photoconductor-type photodetectors and nanosecond response in photodiode-type photodetectors. Through the rational design of material properties and device fabrication techniques, the detectors will be suitable for practical applications in the near future.

Conflicts of interest

The authors declare no conflict of interest.

Acknowledgements

This work is supported by Shandong University, Union Project of Natural Science Foundation of Shandong Province (ZR2016YL020).

Notes and references

1 X. Li, D. Bi, C. Yi, J. D. Decoppet, J. Luo, S. M. Zakeeruddin, A. Hagfeldt and M. Gratzel, *Science*, 2016, **353**, 58–62.
2 J. Burschka, N. Pellet, S.-J. Moon, R. Humphry-Baker, P. Gao, M. K. Nazeeruddin and M. Graetzel, *Nature*, 2013, **499**, 316–319.
3 H. J. Snaith, *J. Phys. Chem. Lett.*, 2013, **4**, 3623–3630.
4 W. S. Yang, B.-W. Park, E. H. Jung, N. J. Jeon, Y. C. Kim, D. U. Lee, S. S. Shin, J. Seo, E. K. Kim, J. H. Noh and S. I. Seok, *Science*, 2017, **356**, 1376–1379.
5 H. Zhou, Q. Chen, G. Li, S. Luo, T.-B. Song, H.-S. Duan, Z. Hong, J. You, Y. Liu and Y. Yang, *Science*, 2014, **345**, 542–546.
6 W. S. Yang, J. H. Noh, N. J. Jeon, Y. C. Kim, S. Ryu, J. Seo and S. I. Seok, *Science*, 2015, **348**, 1234–1237.
7 M. A. Green, A. Ho-Baillie and H. J. Snaith, *Nat. Photonics*, 2014, **8**, 506–514.
8 M. Liu, M. B. Johnston and H. J. Snaith, *Nature*, 2013, **501**, 395–398.
9 W. Chen, Y. Wu, Y. Yue, J. Liu, W. Zhang, X. Yang, H. Chen, E. Bi, I. Ashraful, M. Graetzel and L. Han, *Science*, 2015, **350**, 944–948.
10 X. Zheng, J. Troughton, N. Gasparini, Y. Lin, M. Wei, Y. Hou, J. Liu, K. Song, Z. Chen, C. Yang, B. Turedi, A. Y. Alsalloum, J. Pan, J. Chen, A. A. Zhumekenov, T. D. Anthopoulos, Y. Han, D. Baran, O. F. Mohammed, E. H. Sargent and O. M. Bakr, *Joule*, 2019, **3**, 1963–1976.
11 N. Li, S. Tao, Y. Chen, X. Niu, C. K. Onwudinanti, C. Hu, Z. Qiu, Z. Xu, G. Zheng, L. Wang, Y. Zhang, L. Li, H. Liu, Y. Lun, J. Hong, X. Wang, Y. Liu, H. Xie, Y. Gao, Y. Bai, S. Yang, G. Brocks, Q. Chen and H. Zhou, *Nat. Energy*, 2019, **4**, 408–415.
12 X. Jiang, S. Xia, J. Zhang, D. Ju, Y. Liu, X. Hu, L. Wang, Z. Chen and X. Tao, *ChemSusChem*, 2019, **12**, 5228–5232.
13 Z. Chen, B. Turedi, A. Y. Alsalloum, C. Yang, X. Zheng, I. Gereige, A. AlSaggaf, O. F. Mohammed and O. M. Bakr, *ACS Energy Lett.*, 2019, **4**, 1258–1259.
14 Z. Chen, Q. Dong, Y. Liu, C. Bao, Y. Fang, Y. Lin, S. Tang, Q. Wang, X. Xiao, Y. Bai, Y. Deng and J. Huang, *Nat. Commun.*, 2017, **8**, 1890.
15 X. Jiang, X. Fu, D. Ju, S. Yang, Z. Chen and X. Tao, *ACS Energy Lett.*, 2020, **5**, 1797–1803.
16 Q. Zeng, X. Zhang, C. Liu, T. Feng, Z. Chen, W. Zhang, W. Zheng, H. Zhang and B. Yang, *Sol. RRL*, 2019, **3**, 1800239.
17 X. Zheng, B. Chen, J. Dai, Y. Fang, Y. Bai, Y. Lin, H. Wei, X. C. Zeng and J. Huang, *Nat. Energy*, 2017, **2**, 17102.
18 T. S. Sherkar, C. Momblona, L. Gil-Escrig, J. Ávila, M. Sessolo, H. J. Bolink and L. J. A. Koster, *ACS Energy Lett.*, 2017, **2**, 1214–1222.
19 D. W. deQuilettes, S. M. Vorpahl, S. D. Stranks, H. Nagaoka, G. E. Eperon, M. E. Ziffer, H. J. Snaith and D. S. Ginger, *Science*, 2015, **348**, 683–686.
20 C. Wehrenfennig, G. E. Eperon, M. B. Johnston, H. J. Snaith and L. M. Herz, *Adv. Mater.*, 2014, **26**, 1584–1589.
21 A. Kojima, K. Teshima, Y. Shirai and T. Miyasaka, *J. Am. Chem. Soc.*, 2009, **131**, 6050–6051.
22 National Renewable Energy Laboratory (NREL), Best Research-Cell Efficiencies Chart, https://www.nrel.gov/pv/cell-efficiency.html, accessed June 2020.
23 X. Hu, X. Zhang, L. Liang, J. Bao, S. Li, W. Yang and Y. Xie, *Adv. Funct. Mater.*, 2014, **24**, 7373–7380.
24 J. Feng, C. Gong, H. Gao, W. Wen, Y. Gong, X. Jiang, B. Zhang, Y. Wu, Y. Wu, H. Fu, L. Jiang and X. Zhang, *Nat. Electron.*, 2018, **1**, 404–410.

25 S.-F. Leung, K.-T. Ho, P.-K. Kung, V. K. S. Hsiao, H. N. Alshareef, Z. L. Wang and J.-H. He, *Adv. Mater.*, 2018, **30**, 1704611.
26 W. Wei, Y. Zhang, Q. Xu, H. Wei, Y. Fang, Q. Wang, Y. Deng, T. Li, A. Gruverman, L. Cao and J. Huang, *Nat. Photonics*, 2017, **11**, 315–321.
27 H. Zhu, Y. Fu, F. Meng, X. Wu, Z. Gong, Q. Ding, M. V. Gustafsson, M. T. Trinh, S. Jin and X. Y. Zhu, *Nat. Mater.*, 2015, **14**, 636–642.
28 S. Zou, Y. Liu, J. Li, C. Liu, R. Feng, F. Jiang, Y. Li, J. Song, H. Zeng, M. Hong and X. Chen, *J. Am. Chem. Soc.*, 2017, **139**, 11443–11450.
29 H. Cho, Y.-H. Kim, C. Wolf, H.-D. Lee and T.-W. Lee, *Adv. Mater.*, 2018, **30**, 1704587.
30 T. Xuan, J. Huang, H. Liu, S. Lou, L. Cao, W. Gan, R.-S. Liu and J. Wang, *Chem. Mater.*, 2019, **31**, 1042–1047.
31 Q. Zhang, M. M. Tavakoli, L. Gu, D. Zhang, L. Tang, Y. Gao, J. Guo, Y. Lin, S.-F. Leung, S. Poddar, Y. Fu and Z. Fan, *Nat. Commun.*, 2019, **10**, 727.
32 X. Jiang, Z. Chen and X. Tao, *Front. Chem.*, 2020, **8**, 352.
33 Q. Wang, X. Zheng, Y. Deng, J. Zhao, Z. Chen and J. Huang, *Joule*, 2017, **1**, 371–382.
34 Q. Zeng, X. Zhang, X. Feng, S. Lu, Z. Chen, X. Yong, S. A. T. Redfern, H. Wei, H. Wang, H. Shen, W. Zhang, W. Zheng, H. Zhang, J. S. Tse and B. Yang, *Adv. Mater.*, 2018, **30**, 1705393.
35 Y. Lin, Y. Bai, Y. Fang, Z. Chen, S. Yang, X. Zheng, S. Tang, Y. Liu, J. Zhao and J. Huang, *J. Phys. Chem. Lett.*, 2018, **9**, 654–658.
36 Q. Hu, H. Wu, J. Sun, D. H. Yan, Y. L. Gao and J. L. Yang, *Nanoscale*, 2016, **8**, 5350–5357.
37 C.-W. Chen, H.-W. Kang, S.-Y. Hsiao, P.-F. Yang, K.-M. Chiang and H.-W. Lin, *Adv. Mater.*, 2014, **26**, 6647–6652.
38 J. Zhang, G. Hodes, Z. Jin and S. Liu, *Angew. Chem., Int. Ed.*, 2019, **58**, 15596–15618.
39 Q. Jiang, Y. Zhao, X. Zhang, X. Yang, Y. Chen, Z. Chu, Q. Ye, X. Li, Z. Yin and J. You, *Nat. Photonics*, 2019, **13**, 460–466.
40 Y. Bai, Y. Lin, L. Ren, X. Shi, E. Strounina, Y. Deng, Q. Wang, Y. Fang, X. Zheng, Y. Lin, Z.-G. Chen, Y. Du, L. Wang and J. Huang, *ACS Energy Lett.*, 2019, **4**, 1231–1240.
41 X. Cheng, S. Yang, B. Q. Cao, X. T. Tao and Z. L. Chen, *Adv. Funct. Mater.*, 2020, **30**, 1905021.
42 G. E. Eperon, V. M. Burlakov, P. Docampo, A. Goriely and H. J. Snaith, *Adv. Funct. Mater.*, 2014, **24**, 151–157.
43 E. Aydin, M. De Bastiani and S. De Wolf, *Adv. Mater.*, 2019, **31**, 1900428.
44 M. L. Agiorgousis, Y.-Y. Sun, H. Zeng and S. Zhang, *J. Am. Chem. Soc.*, 2014, **136**, 14570–14575.
45 Q. Wang, B. Chen, Y. Liu, Y. Deng, Y. Bai, Q. Dong and J. Huang, *Energy Environ. Sci.*, 2017, **10**, 516–522.
46 J. Ding, S. Du, T. Zhou, Y. Yuan, X. Cheng, L. Jing, Q. Yao, J. Zhang, Q. He, H. Cui, X. Zhan and H. Sun, *J. Phys. Chem. C*, 2019, **123**, 14969–14975.
47 L. Jing, X. Cheng, Y. Yuan, S. Du, J. Ding, H. Sun, X. Zhan and T. Zhou, *J. Phys. Chem. C*, 2019, **123**, 10826–10830.
48 J. Huang, Y. Shao and Q. Dong, *J. Phys. Chem. Lett.*, 2015, **6**, 3218–3227.
49 Z. Chen, C. Li, A. A. Zhumekenov, X. Zheng, C. Yang, H. Yang, Y. He, B. Turedi, O. F. Mohammed, L. Shen and O. M. Bakr, *Adv. Opt. Mater.*, 2019, **7**, 1900506.
50 Q. Han, S.-H. Bae, P. Sun, Y.-T. Hsieh, Y. Yang, Y. S. Rim, H. Zhao, Q. Chen, W. Shi, G. Li and Y. Yang, *Adv. Mater.*, 2016, **28**, 2253–2258.
51 Z. Lian, Q. Yan, T. Gao, J. Ding, Q. Lv, C. Ning, Q. Li and J.-l. Sun, *J. Am. Chem. Soc.*, 2016, **138**, 9409–9412.
52 Y. Liu, Z. Yang, D. Cui, X. Ren, J. Sun, X. Liu, J. Zhang, Q. Wei, H. Fan, F. Yu, X. Zhang, C. Zhao and S. Liu, *Adv. Mater.*, 2015, **27**, 5176–5183.
53 Y. Liu, Y. Zhang, K. Zhao, Z. Yang, J. Feng, X. Zhang, K. Wang, L. Meng, H. Ye, M. Liu and S. Liu, *Adv. Mater.*, 2018, **30**, 1707314.
54 W. Peng, X. Miao, V. Adinolfi, E. Alarousu, O. El Tall, A.-H. Emwas, C. Zhao, G. Walters, J. Liu, O. Ouellette, J. Pan, B. Murali, E. H. Sargent, O. F. Mohammed and O. M. Bakr, *Angew. Chem., Int. Ed.*, 2016, **55**, 10686–10690.
55 F. Zhang, B. Yang, X. Mao, R. Yang, L. Jiang, Y. Li, J. Xiong, Y. Yang, R. He, W. Deng and K. Han, *ACS Appl. Mater. Interfaces*, 2017, **9**, 14827–14832.
56 A. A. Zhumekenov, M. I. Saidaminov, M. A. Haque, E. Alarousu, S. P. Sarmah, B. Murali, I. Dursun, X.-H. Miao, A. L. Abdelhady, T. Wu, O. F. Mohammed and O. M. Bakr, *ACS Energy Lett.*, 2016, **1**, 32–37.
57 Y. Cheng, S. Liu, L. Wang, G. Liu, P. Zhao, M. Lin, K. Sui and H. Zhang, *Compos. Commun.*, 2020, **20**, 100342.
58 Q. Dong, Y. Fang, Y. Shao, P. Mulligan, J. Qiu, L. Cao and J. Huang, *Science*, 2015, **347**, 967–970.
59 L. Chen, Y.-Y. Tan, Z.-X. Chen, T. Wang, S. Hu, Z.-A. Nan, L.-Q. Xie, Y. Hui, J.-X. Huang, C. Zhan, S.-H. Wang, J.-Z. Zhou, J.-W. Yan, B.-W. Mao and Z.-Q. Tian, *J. Am. Chem. Soc.*, 2019, **141**, 1665–1671.
60 H. Wei, Y. Fang, P. Mulligan, W. Chuirazzi, H.-H. Fang, C. Wang, B. R. Ecker, Y. Gao, M. A. Loi, L. Cao and J. Huang, *Nat. Photonics*, 2016, **10**, 333–339.
61 F. Zhang, B. Yang, K. Zheng, S. Yang, Y. Li, W. Deng and R. He, *Nano-Micro Lett.*, 2018, **10**, 43.
62 D. Shi, V. Adinolfi, R. Comin, M. J. Yuan, E. Alarousu, A. Buin, Y. Chen, S. Hoogland, A. Rothenberger, K. Katsiev, Y. Losovyj, X. Zhang, P. A. Dowben, O. F. Mohammed, E. H. Sargent and O. M. Bakr, *Science*, 2015, **347**, 519–522.
63 Y. Dang, Y. Liu, Y. Sun, D. Yuan, X. Liu, W. Lu, G. Liu, H. Xia and X. Tao, *CrystEngComm*, 2015, **17**, 665–670.
64 Z. Lian, Q. Yan, Q. Lv, Y. Wang, L. Liu, L. Zhang, S. Pan, Q. Li, L. Wang and J. L. Sun, *Sci. Rep.*, 2015, **5**, 16563.
65 M. I. Saidaminov, V. Adinolfi, R. Comin, A. L. Abdelhady, W. Peng, I. Dursun, M. Yuan, S. Hoogland, E. H. Sargent and O. M. Bakr, *Nat. Commun.*, 2015, **6**, 8724.
66 C. Bao, Z. Chen, Y. Fang, H. Wei, Y. Deng, X. Xiao, L. Li and J. Huang, *Adv. Mater.*, 2017, **29**, 1703209.
67 H. Wang and D. H. Kim, *Chem. Soc. Rev.*, 2017, **46**, 5204–5236.
68 M. I. Saidaminov, M. A. Haque, M. Savoie, A. L. Abdelhady, N. Cho, I. Dursun, U. Buttner, E. Alarousu, T. Wu and O. M. Bakr, *Adv. Mater.*, 2016, **28**, 8144–8149.

69 V. Adinolfi, O. Ouellette, M. I. Saidaminov, G. Walters, A. L. Abdelhady, O. M. Bakr and E. H. Sargent, *Adv. Mater.*, 2016, **28**, 7264–7268.
70 Z. Yang, Y. Deng, X. Zhang, S. Wang, H. Chen, S. Yang, J. Khurgin, N. X. Fang, X. Zhang and R. Ma, *Adv. Mater.*, 2018, **30**, 1704333.
71 Y. Lin, Y. Bai, Y. Fang, Q. Wang, Y. Deng and J. Huang, *ACS Energy Lett.*, 2017, **2**, 1571–1572.
72 Y. Liu, Y. Zhang, Z. Yang, H. Ye, J. Feng, Z. Xu, X. Zhang, R. Munir, J. Liu, P. Zuo, Q. Li, M. Hu, L. Meng, K. Wang, D. M. Smilgies, G. Zhao, H. Xu, Z. Yang, A. Amassian, J. Li, K. Zhao and S. F. Liu, *Nat. Commun.*, 2018, **9**, 5302.
73 G. Maculan, A. D. Sheikh, A. L. Abdelhady, M. I. Saidaminov, M. A. Haque, B. Murali, E. Alarousu, O. F. Mohammed, T. Wu and O. M. Bakr, *J. Phys. Chem. Lett.*, 2015, **6**, 3781–3786.
74 M. I. Saidaminov, M. A. Haque, J. Almutlaq, S. Sarmah, X.-H. Miao, R. Begum, A. A. Zhumekenov, I. Dursun, N. Cho, B. Murali, O. F. Mohammed, T. Wu and O. M. Bakr, *Adv. Opt. Mater.*, 2017, **5**, 1600704.
75 Y. Fang, Q. Dong, Y. Shao, Y. Yuan and J. Huang, *Nat. Photonics*, 2015, **9**, 679–686.
76 X. Xiao, C. Bao, Y. Fang, J. Dai, B. R. Ecker, C. Wang, Y. Lin, S. Tang, Y. Liu, Y. Deng, X. Zheng, Y. Gao, X. C. Zeng and J. Huang, *Adv. Mater.*, 2018, **30**, 1705176.
77 H. Wei and J. Huang, *Nat. Commun.*, 2019, **10**, 1066.
78 W. Pan, H. Wu, J. Luo, Z. Deng, C. Ge, C. Chen, X. Jiang, W.-J. Yin, G. Niu, L. Zhu, L. Yin, Y. Zhou, Q. Xie, X. Ke, M. Sui and J. Tang, *Nat. Photonics*, 2017, **11**, 726–732.
79 Y. Liu, Z. Xu, Z. Yang, Y. Zhang, J. Cui, Y. He, H. Ye, K. Zhao, H. Sun, R. Lu, M. Liu, M. Kanatzidis and S. L. Frank Liu, *Matter*, 2020, **3**, 1–17.
80 M. Xia, J.-H. Yuan, G. Niu, X. Du, L. Yin, W. Pan, J. Luo, Z. Li, H. Zhao, K.-H. Xue, X. Miao and J. Tang, *Adv. Funct. Mater.*, 2020, **30**, 1910648.
81 Y. Zhang, Y. Liu, Z. Xu, H. Ye, Z. Yang, J. You, M. Liu, Y. He, M. G. Kanatzidis and S. Liu, *Nat. Commun.*, 2020, **11**, 2304.
82 J. Ding, L. Jing, X. Cheng, Y. Zhao, S. Du, X. Zhan and H. Cui, *J. Phys. Chem. Lett.*, 2018, **9**, 216–221.
83 Y. Liu, J. Sun, Z. Yang, D. Yang, X. Ren, H. Xu, Z. Yang and S. Liu, *Adv. Opt. Mater.*, 2016, **4**, 1829–1837.

